Journal of Crystal Growth 630 (2024) 127592

Contents lists available at ScienceDirect

Journal of Crystal Growth

journal homepage: www.elsevier.com/locate/jcrysgro

Crystal growth and Hall effect of the non-centrosymmetric superconductor α-BiPd and the topological superconductor β-Bi_2Pd

Raja Arumugam [a,1], Rosalba Fittipaldi [a,1,*], Anita Guarino [a,*], Daniel Mayoh [b], Alberto Ubaldini [c], Mariateresa Lettieri [a], Guerino Avallone [d], Alfonso Romano [d], Geetha Balakrishnan [b], Antonio Vecchione [a]

[a] CNR-SPIN, c/o University of Salerno, Via Giovanni Paolo II, 132, I-84084 Fisciano, Salerno, Italy
[b] Department of Physics, University of Warwick, Coventry CV4 7AL, United Kingdom
[c] ENEA, Bologna Research Centre, Bologna, 40129, Italy
[d] Department of Physics, University of Salerno, I-84084 Fisciano, Salerno, Italy

ARTICLE INFO

Communicated by Chennai Guest Editor

Keywords:
A2. Single crystal growth
A2. Floating zone technique
A1. Crystal morphology
A1. Crystal structure
B1. Alloys
B2. Superconducting materials

ABSTRACT

Due to the rarity of triplet pairing, topological superconductors (SCs) have primarily been realized experimentally in manufactured topological phases, such as heterostructures, where the proximity effect causes triplet pairing with traditional s-wave SCs. Recently, there has been a lot of interest in investigating novel quantum materials with spin-triplet pairs in order to develop Majorana physics and creating quantum computers. Bi-based superconductors are speculated to hold promise for realizing spin-triplet pairing due to its large spin orbit coupling. In this work, we present the growth of α-BiPd and β-Bi_2Pd single crystals using the optical floating zone technique and their characterization. The single crystals of α-BiPd and β-Bi_2Pd are found to crystallize in monoclinic and tetragonal crystalline system with space group $P2_1$ and *I*4/mmm, respectively. The composition and microstructure of the grown crystals were analyzed with a scanning electron microscope, through energy dispersive spectroscopy (EDS) and electron backscattered diffraction (EBSD) analysis. The superconducting behavior and Hall effect of both α-BiPd and β-Bi_2Pd single crystals have been investigated through resistivity measurements.

1. Introduction

Recently, there has been a lot of interest in investigating novel materials with quantum behaviors in order to create quantum computing devices. Superconductor-based qubits have emerged as one of the top contenders for scalable quantum processors among them [1,2]. Cooper pairs are created when two electrons condense, producing superconductivity. Cooper pairs can either be spin singlet (S = 0) with an even parity gap or spin-triplet (S = 1) with an odd parity gap in superconductors (SCs). The majority of known SCs are singlet, primarily s-wave, with some d-wave. Although extremely uncommon, triplet SCs with p-wave pairs are crucial for Majorana physics and quantum computing.

Triplet pairing is rare, so topological SCs have been experimentally produced largely utilizing synthetic topological phases, such as heterostructures, where the proximity effect leads to triplet pairing with conventional s-wave SCs. Recent studies, however, have demonstrated that singlet s-wave SC-based detection strategies merely exacerbate confusion and are difficult to implement [3,4]. For devices that can look at the potential Majorana bound modes, intrinsic triplet p-wave SCs are necessary.

It is well known that the inversion symmetry requires the centrosymmetric SCs to be either even-parity singlets or odd-parity triplets. However, superconductivity in non-centrosymmetric SCs without inversion symmetry can be a mix of singlet and triplet pairing. Materials lacking inversion symmetry are ideal for discovering triplet SCs. This has motivated intensive research activity in recent years on Bi-Pd alloys, which can form both the non-centrosymmetric α-BiPd superconductor and the topological β-Bi_2Pd superconductor.

Concerning α-BiPd, it exhibits a monoclinic structure and then undergoes the transition to the superconducting phase at Tc = 3.7 K [5].

* Corresponding authors.
E-mail addresses: rosalba.fittipaldi@spin.cnr.it (R. Fittipaldi), anita.guarino@spin.cnr.it (A. Guarino).
[1] Contributed equally.

https://doi.org/10.1016/j.jcrysgro.2024.127592
Received 9 November 2023; Received in revised form 10 January 2024; Accepted 17 January 2024
Available online 19 January 2024

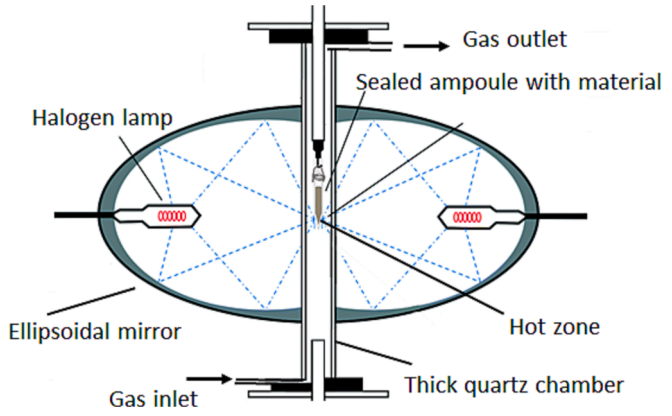

Fig. 1. A sketch of modified FZ technique with material loaded and melted in a sealed tip-shaped quartz tube.

Based on point contact Andreev reflection [6] and penetration depth measurements [7], it has been proposed that the superconducting phase is characterized by a two-gap structure, with one gap fully open, and the second gap highly anisotropic and changing sign across the Fermi surface. This is consistent with the fact that the electric field gradient present in a crystal with no inversion symmetry originates an antisymmetric spin–orbit coupling which may lift the spin degeneracy, splitting the related bands and allowing the mixture of spin-singlet and spin-triplet states. ARPES spectroscopy [8–11], phase-sensitive experiments [12] as well as ab initio electronic band structure calculations seem to confirm the above-mentioned scenario, which has also been shown to be accompanied by the presence of surface states with Dirac-like dispersion. On the other hand, other experiments such as scanning tunneling spectroscopy [13] and upper critical field measurements [14] gave indication of a predominately singlet s-wave superconductivity with a nodeless single gap. In these cases, the absence of a triplet component in the order parameter led to the hypothesis that the parity-breaking spin–orbit coupling induced by noncentrosymmetry is maybe too weak to give rise to observable effects, so the need for further verification of the two-band scenario was invoked.

Differently from α-BiPd, β-Bi_2Pd is a compound with centrosymmetric tetragonal crystal structure, often considered as a possible candidate for topological superconductivity, that is, a phase characterized by a full pairing gap in the bulk and topologically protected gapless states on the surface. Nonetheless, the results about the origin of the superconducting phase which develops below Tc = 5.4 K [15–17] are still controversial, given that for this system there are indications of a multigap superconductivity [15], of topologically protected surface states [16,18,19], as well as of a standard conventional s-wave pairing [17,20–22]. While α-BiPd appears to be topologically trivial, the structure of the superconducting gap and the role of the topologically protected surface states in the superconducting pairing mechanism of β-Bi_2Pd still remain to be clarified.

The still open questions outlined above make it evident that experiments on α-BiPd and β-Bi_2Pd need to be carried out on high-quality single crystals. Their preparation and characterization represents the subject of our investigation. In particular, we describe the detailed synthesis and crystal growth of these two systems, realized by floating zone technique, together with their structural, compositional, and electrical properties, both in the superconducting and normal state.

2. Experimental

The individual elements of Bismuth (Bi) and Palladium (Pd) were weighed in accordance with the stoichiometric ratio of 1:1 mol% of Bi and Pd, and 2:1 mol% of Bi and Pd to get the crystals BiPd and Bi_2Pd, respectively. The weighed materials were loaded in a quartz tube with a cone-shaped end (ampoule). Before filling it with materials, the quartz tube was cleaned with ethanol and dried. Once filled with pieces of Bi (Alfa Aesar, 99.997 %) and Pd (Aldrich, 99.99 %) in an appropriate stoichiometric ratio, the ampoule was sealed with vacuum level of 2×10^{-6} mbar. Before sealing, the quartz tube was purged with argon for four times. Once sealed, the ampoule was placed in the box furnace for the following thermal treatment: the temperature was increased from room temperature to 680 °C at the rate of 50 °C per hour and kept for 12 h, then the furnace was cooled to room temperature at the rate of 20 °C per hour. After thermal treatment in the box furnace, the ampoules with synthesized BiPd and Bi_2Pd were placed vertically in a two-mirror optical image furnace (NEC Machinery, model SC1-MDH11020). Single crystals of BiPd and Bi_2Pd were grown using the Optical Floating Zone (FZ) technique with a high temperature gradient [23].

In particular, a modified FZ technique, developed in the last few years to synthetize crystals not containing oxygen, such as the semiconductor CdS [24] and various topological insulators such as $Pb_{0.5}Sn_{0.5}Te$ [25] and $Bi_{1.33}Sb_{0.67}Se_3$ [26], has been adopted. The set up for the modified FZ experiments is shown in Fig. 1. The material in the bottom (tip) of the quartz ampoule is melted by the power of the halogen lamps focused on the sample placed in the focal point of the ellipsoidal mirrors, while the halogen lamps of appropriate power sit at the other focal points of the two mirrors.

This configuration results in a steep temperature gradient. To grow the BiPd and Bi_2Pd crystals, the ampoule was lowered downward at a constant growth speed $v_g = 0.5$ mm/h and was kept rotated at 20 rpm during the whole growth process, Fig. 2(a). Furthermore, a continuous flow of argon at a rate of 0.25 l/min was applied to the outer quartz tube.

Phase formation and purity of the synthesized crystals were analyzed by x-ray diffraction using a Bruker D2 PHASER 2nd generation with CuK_α radiation of 1.54 Å. Elemental composition analysis of the grown

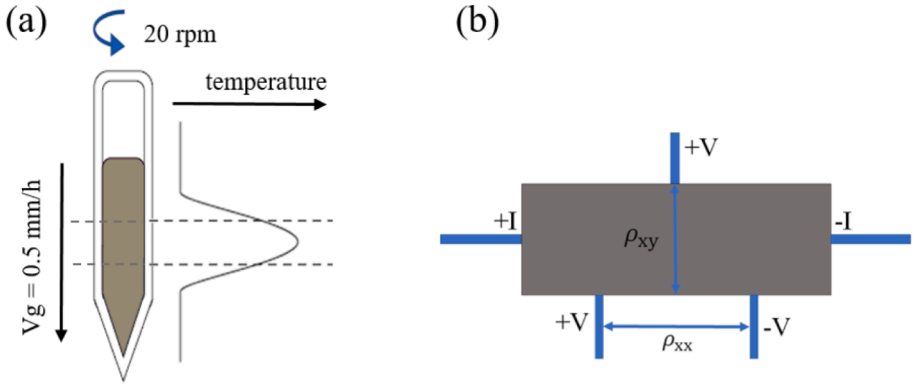

Fig. 2. (a) A sketch of growth process for Bi-Pd single crystals. Molten BiPd or Bi_2Pd was cooled through its melting point in a high temperature gradient while sealed in a quartz tube. (b) A schematic of the 5-point wire configuration used for the longitudinal and Hall resistivity measurements.

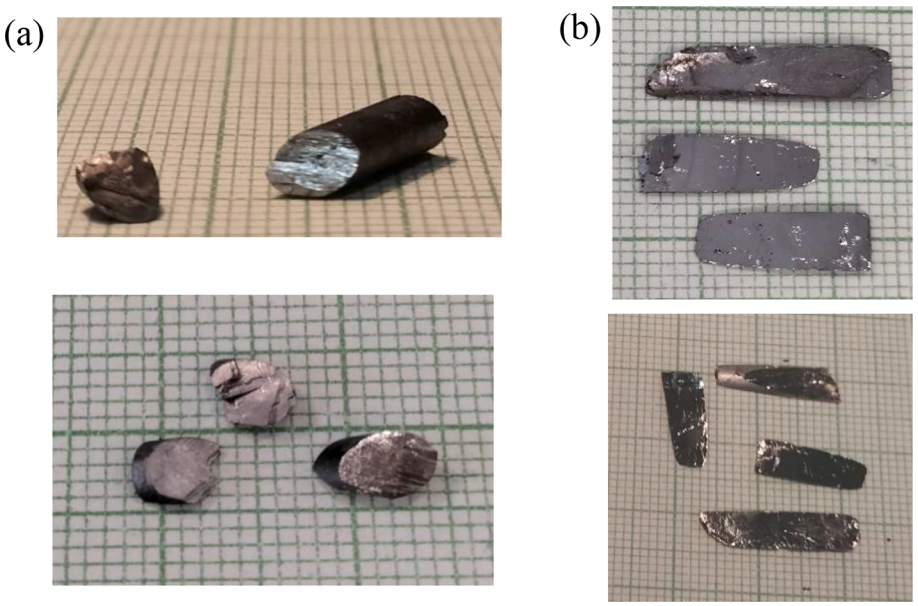

Fig. 3. Pictures of (a) crystal boule, and cleaved pieces of BiPd crystals and (b) cleaved Bi_2Pd crystals.

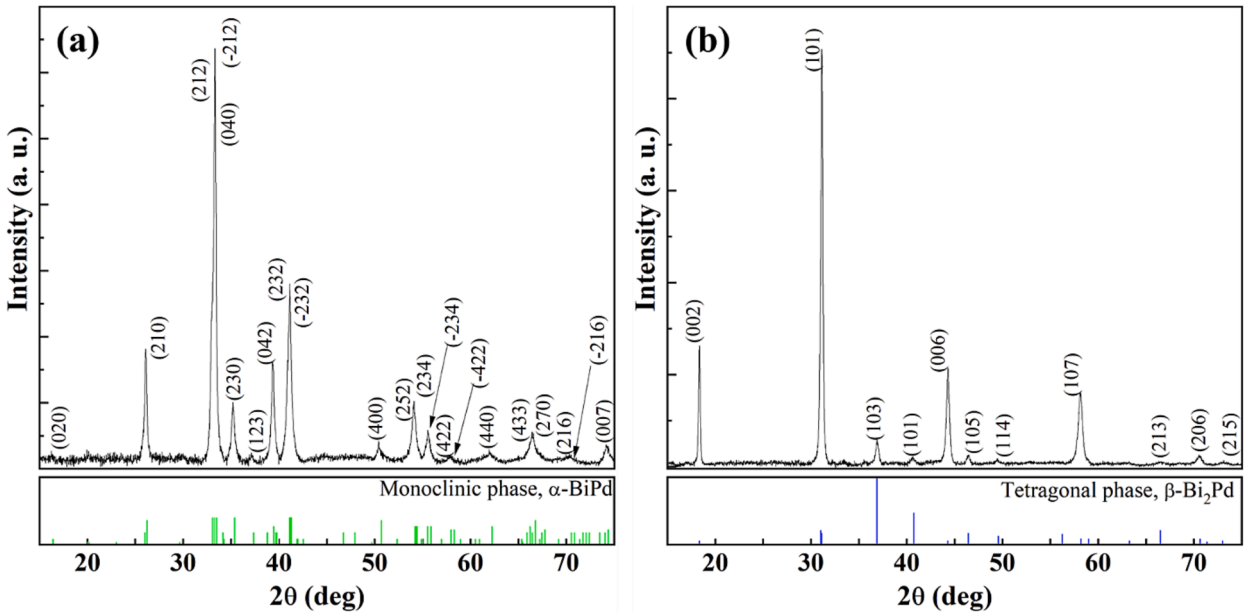

Fig. 4. X-ray diffraction data acquired on powders obtained from grinding (a) BiPd and (b) Bi_2Pd crystals. The pattern (green and blue) below each diffractogram corresponds to the reference pattern obtained using X'Pert HighScore software. (For interpretation of the references to color in this figure legend, the reader is referred to the web version of this article.)

crystals was performed using energy dispersive spectroscopy (EDS) inside a scanning electron microscope (SEM), LEO model EVO 50. Furthermore, electron back-scattered diffraction (EBSD) measurements were carried out on different as-grown cleaved crystals of both BiPd and Bi_2Pd to analyze the sample crystallinity and in plane microstructure. The EBSD measurements were performed using an Inca Crystal 300 EBSD system added to the SEM with a LaB6 gun. During EBSD measurements, the SEM was used with an aperture size of 30 μm, a working distance of 18 mm, an accelerating voltage of 20 kV and a probe current of 5nA. Finally, electronic transport measurements were carried out using the ac resistivity option on a Quantum Design Physical Properties Measurement System (PPMS) with a temperature range from 1.8 to 300 K and applied fields up to 9 T. Hall effect measurements were carried out using a 5-point configuration shown in Fig. 1(b). Longitudinal resistivity data have been symmetrised to remove any field dependence caused by transverse resistivity contributions from contact misalignment.

3. Results and discussion

The pictures of as grown crystals of both BiPd and Bi_2Pd synthetized by FZ technique are shown in Fig. 3 (a) and (b), respectively.

Powder x-ray diffraction (XRD) was used to characterize the phase purity as well as the symmetry of grown crystals. XRD analysis was carried out on powders obtained from grinding both α-BiPd and β-Bi_2Pd crystals, see Fig. 4. The diffractograms were analysed with X'Pert HighScore software and matched with a corresponding reference pattern (green and blue patterns at the bottom of the two panels of Fig. 4). A number of reflections in the experimental patterns do not match the

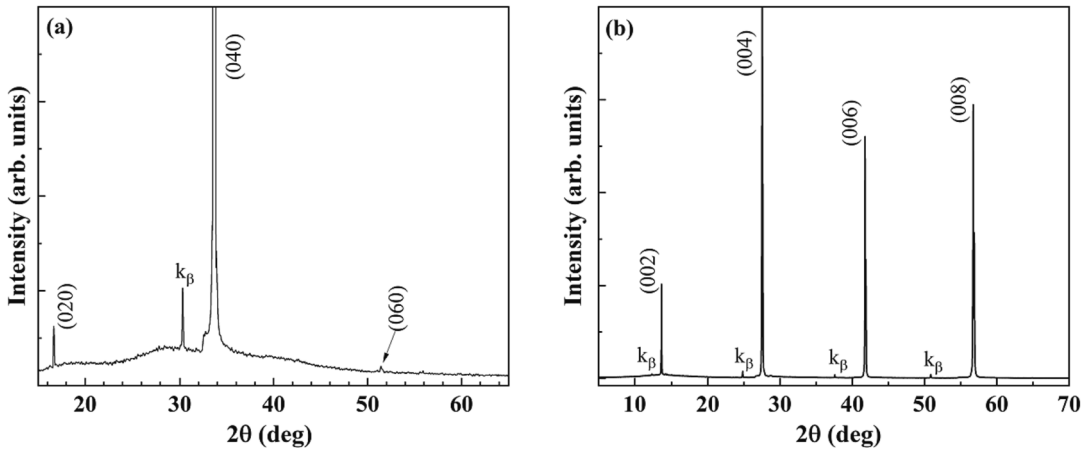

Fig. 5. X-ray diffraction diffractograms acquired on cleaved surface of BiPd crystals (a) and Bi_2Pd crystals (b). The peaks labelled as k_β are the reflections due to the CuK_β radiation.

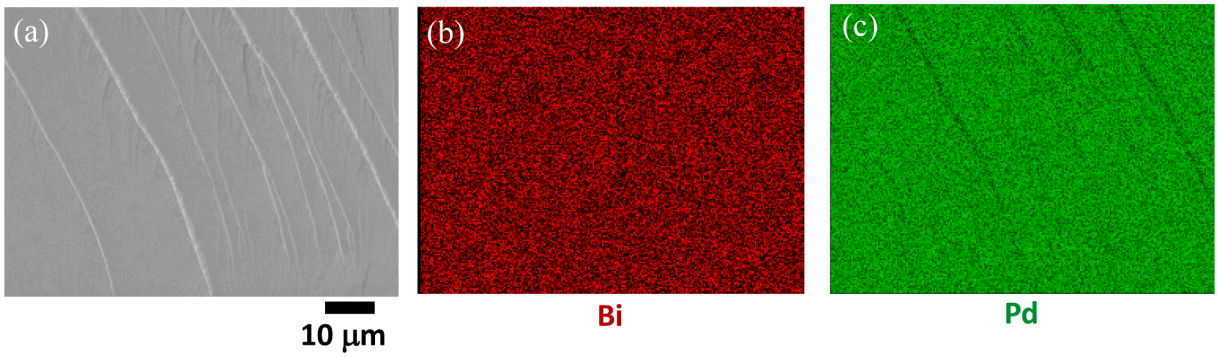

Fig. 6. SEM image (a), and EDS elemental maps for bismuth (b), and palladium (c) of a cleaved surface of α-BiPd crystal.

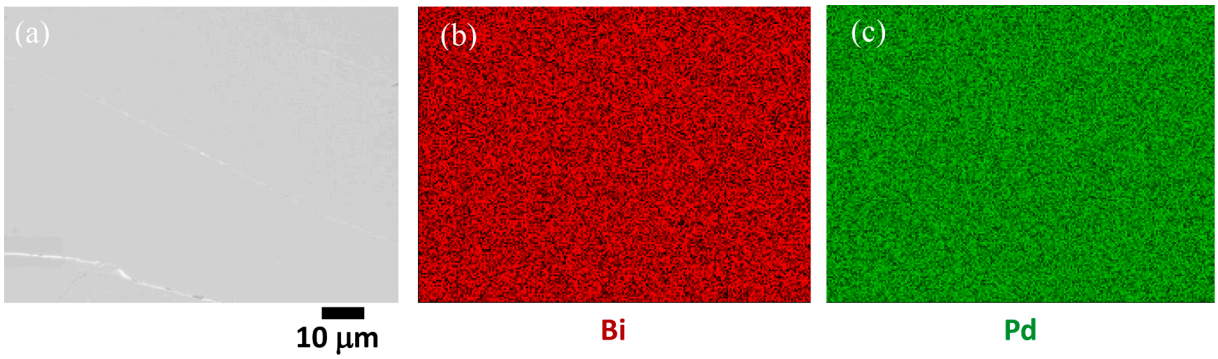

Fig. 7. SEM image of a cleaved surface of β-Bi_2Pd crystal (a), and EDS maps of the corresponding area for bismuth (b), and palladium (c) elements.

intensities of the reference pattern. That is specifically observed in the case of the Bi_2Pd crystals, a layered material that tends to cleave easily forming thin flakes, so it required a great care to be finely ground.

Diffraction peaks in panel (a), obtained by powdered BiPd crystals, can be indexed to the monoclinic α-BiPd structure, with space group $P2_1$ [27], while all the peaks in panel (b), related to XRD analysis performed on powdered Bi_2Pd crystals, correspond to the body-centered tetragonal crystalline structure with the space group I4/mmm [28]. It is worth mentioning that no impurities have been detected for both BiPd and Bi_2Pd samples.

Furthermore, it is remarkable that both types of crystals cleave readily. While the Bi_2Pd crystals show large, shine, and flat cleaved surfaces, the BiPd cleaved crystals exhibit rough surfaces and sometimes internally cracked regions due to the α-β phase transition.

XRD performed on the cleaved surface of the single crystals of BiPd and Bi_2Pd has been used to demonstrate the crystalline nature of the samples, as shown in Fig. 5. The XRD diffractogram in the Fig. 5(a) shows reflections from the (0 k 0) planes only of the monoclinic phase α-BiPd, [27]. This result indicates that the cleaved surface of the produced α-BiPd crystals is perpendicular to the *b*-axis of its monoclinic structure, as found previously [8,29–31].

Regarding the XRD study of freshly cleaved β-Bi_2Pd, only reflections associated with the (0 0 l) planes for the expected tetragonal structure [28] are observed (Fig. 5(b)) indicating that the cleave is along the (h k 0) plane, in agreement with the results of Xu et al. [32].

The phase purity of the two crystals was further confirmed by EDS

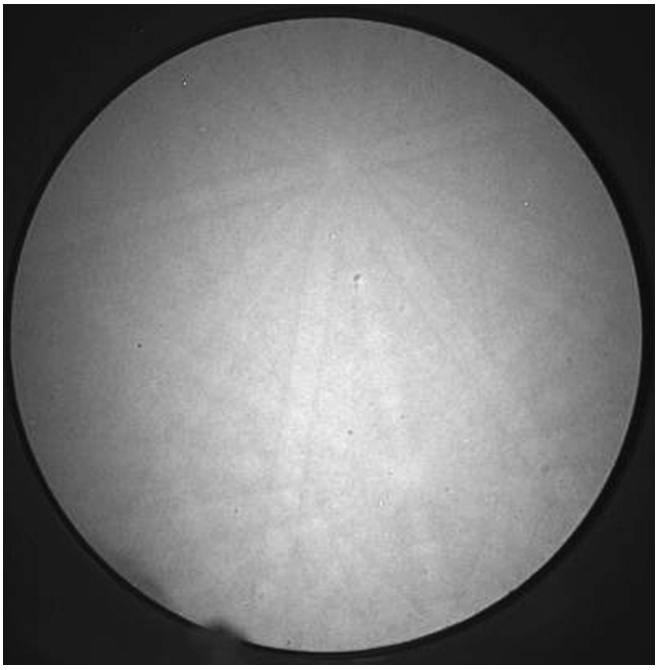

Fig. 8. Kikuchi Electron diffraction pattern collected on the crystalline cleaved surface of an α-BiPd crystal.

compositional maps. Panels (b) and (c) of Figs. 6 and 7 show the elemental maps acquired on cleaved surfaces of α-BiPd and β-Bi_2Pd crystals, respectively. In Fig. 6(b-c) EDS map acquired on BiPd crystal shows a homogeneous distribution of bismuth and palladium corresponding to the composition $Bi_{1.04}Pd_{0.96}$.

Similarly, EDS maps acquired on β-Bi_2Pd crystals (Fig. 7) display a homogeneous composition of $Bi_{1.93}Pd_{1.07}$.

Additionally, a different occurrence of step edges on the surface of cleaved α-BiPd and β-Bi_2Pd crystals has been observed, as especially evidenced by SEM images. This can be noticeably observed comparing, for example, the images reported in panel (a) of Figs. 6 and 7. It is visible that the cleaved surface of α-BiPd crystal exhibits a large number of step edges on the surface (Fig. 6(a)). This feature, due to the layered crystal structure of α-BiPd with an easy-cleavage (0 1 0) plane which favors the occurrence of step edges, was very recently hypothesized by Juraszek et al. [33]. The presence of step edges in α-BiPd crystals grown by Bridgman–Stockbarger technique was also observed by scanning tunneling microscopy by Yim et al [34] and by Sun et al. [13]. In this work, through SEM images it has been possible to spot the presence of many step edges on α-BiPd crystals synthesized by FZ method.

To better clarify the microstructure, the crystallinity, and the in-plane orientation of α-BiPd and β-Bi_2Pd crystals grown by FZ technique, SEM imaging combined with EBSD [35] was carried out. Through EBSD technique the electron beam scans a selected area of the sample, and for the crystalline regions of the sample Kikuchi electron diffraction patterns [36] are generated. During EBSD analysis, the sample was typically tilted at 70° to the horizontal plane to optimize both the contrast in the diffraction pattern and the fraction of electrons scattered from the sample.

It is worth mentioning that high-quality Kikuchi diffraction patterns were observed for both α-BiPd and β-Bi_2Pd crystals only on freshly cleaved surfaces. The crystal surfaces used for EBSD measurements were obtained by cleavage in air and after that rapidly inserted in the SEM vacuum chamber to be kept at a pressure of 10^{-6} mbar. The Kikuchi electron diffraction pattern observed on a smooth α-BiPd surface is shown in Fig. 8.

Fig. 9(a) shows a SEM image of a cleaved surface of α-BiPd crystal on which EBSD mapping has been performed. The EBSD orientation maps of the surface bounded by the dashed line, Fig. 9(b), report the orientation of the α-BiPd crystalline cell along the three directions normal (ND), rolling (RD), and transverse (TD) with respect to the sample surface and orthogonal to each other (see sketch at the bottom right of Fig. 9(a)).

The EBSD orientation maps show a uniform color for the ND and RD, while in the TD two colors are clearly visible. This non-uniform color represents a different crystalline cell orientation, and in particular corresponds to regions with antiparallel orientations of the crystallographic *b*-axis. As described in the panels (1) and (2) of Fig. 9, the blue domains are characterized by a (0 1 0) termination, while the green ones expose a (0 $\bar{1}$ 0) termination.

Similar type of twin boundaries has been observed also in α-BiPd crystals grown with a different technique [10,13,34].

Excellent crystalline quality has been observed on freshly cleaved flat surface of β-Bi_2Pd crystals, similar to what is observed in α-BiPd, and is shown in Fig. 10(a). Moreover, in the case of β-Bi_2Pd crystals the EBSD measurements exhibited that they cleave along (0 0 1) planes, i.e with the *c*-axis orthogonal to the cleaved plane. In all the inspected samples a uniform orientation has been observed, without the presence of grain boundaries. An example of SEM image and EBSD orientation maps acquired on cleaved surface of β-Bi_2Pd crystal is shown in Fig. 10(b) and (c). From the EBSD orientation maps in Fig. 10(c), an orientation of the

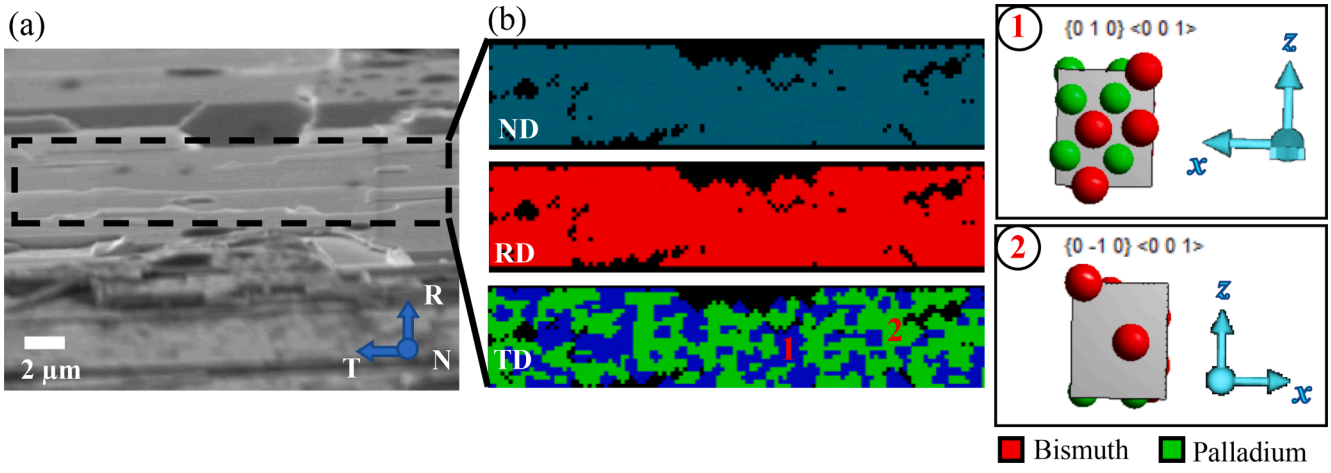

Fig. 9. (a) SEM image and (b) corresponding EBSD orientation maps of an α-BiPd crystal. Panels (1) and (2) report the crystalline cell pictures of the α-BiPd phase as inferred by EBSD orientation maps in panel (b). In particular, panels (1) and (2) refer to the blue domains (denoted with 1) and the green domains (labelled as 2) in the TD map. (For interpretation of the references to color in this figure legend, the reader is referred to the web version of this article.)

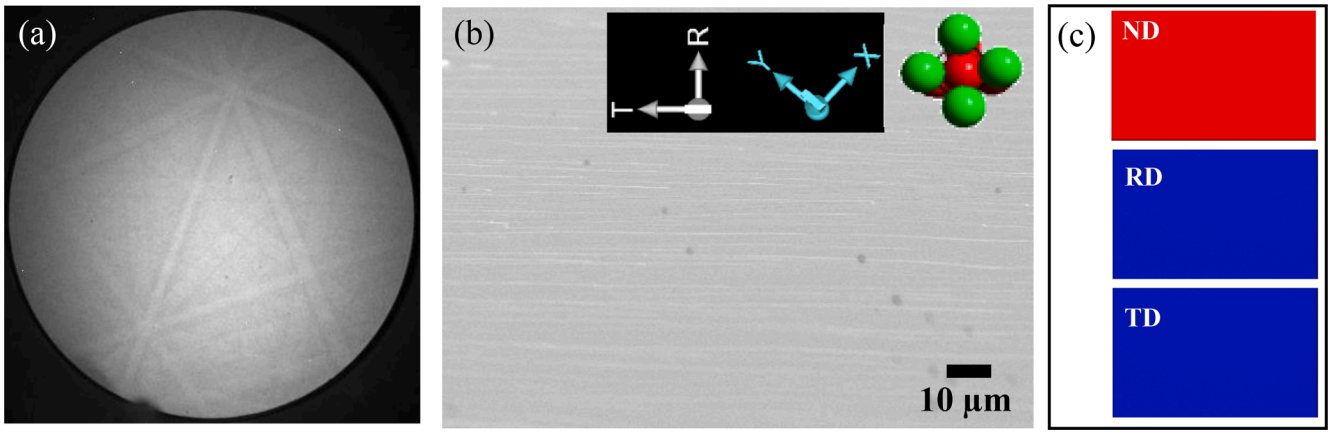

Fig. 10. (a) Kikuchi electron diffraction pattern collected on the crystalline cleaved surface of β-Bi_2Pd crystal, (b) SEM image of cleaved β-Bi_2Pd crystal and its crystallographic cell orientation inferred by EBSD orientation maps; (c) EBSD orientation maps acquired along the normal (ND), rolling (RD) and transverse (TD) directions on the surface in panel (b). The atoms labels in the inset of Fig. 8(b) are bismuth red, and palladium green. (For interpretation of the references to color in this figure legend, the reader is referred to the web version of this article.)

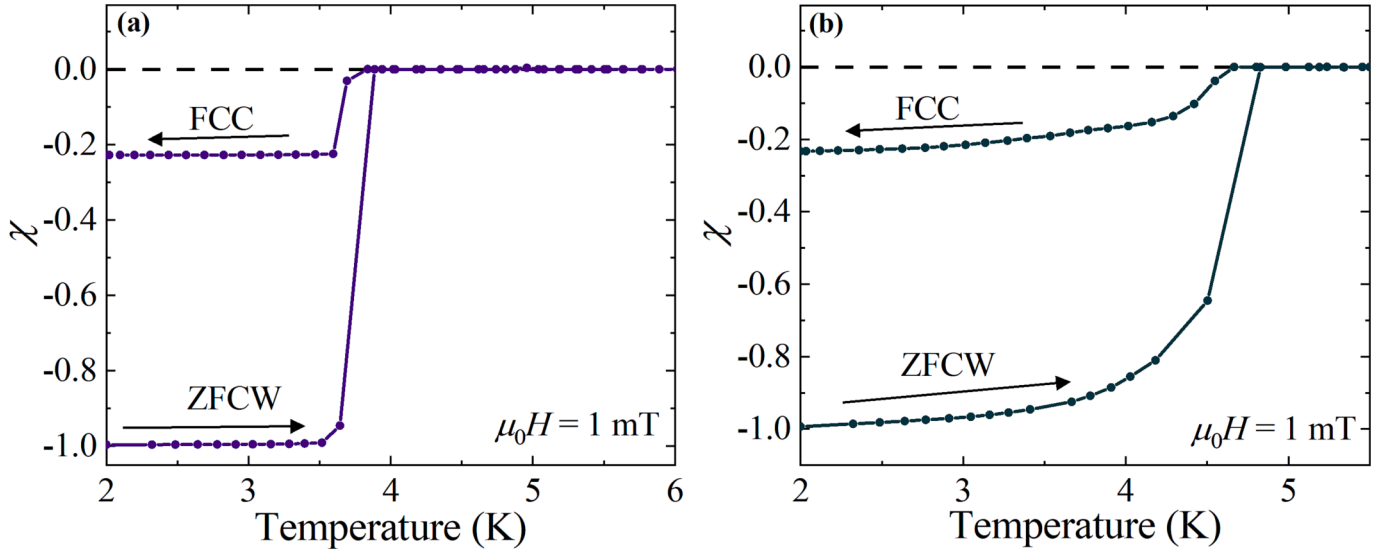

Fig. 11. Magnetic susceptibility as a function of temperature for (a) α-BiPd and (b) β-Bi_2Pd in an applied field of 1 mT, collected in zero-field cooled warming (ZFCW) and field-cooled cooling (FCC) modes.

β-Bi_2Pd crystalline cell can be inferred with the *c*-axis pointing out to the examined surface while *a* and *b*-axis are placed at 45° with respect to the edges of the analysed crystal piece (see the inset of Fig. 10(a)).

To gain insight into the superconducting behaviour of both α-BiPd and β-Bi_2Pd crystals, measurements of the magnetic susceptibility χ as a function of temperature have been performed (Fig. 11). The data were collected in zero-field-cooled warming (ZFCW) and field-cooled cooling (FCC) mode in a field of 1 mT applied perpendicular to the cleaved plane. A full Meissner fraction for both systems is seen in the ZFCW mode while some flux expulsion is observed in the FCC. These data confirm that superconductivity arises in both BiPd and Bi_2Pd at the critical temperatures $T_c = 3.87(5)$ K and 4.82(5) K, respectively.

The superconducting transition in both systems is also made evident by the behavior of the transverse resistivity ρ_{xx} shown in Fig. 12 as a function of temperature. For both α-BiPd and β-Bi_2Pd ρ_{xx} has a typical metallic behavior, with a monotonous decrease to a plateau developing before the transition to the superconducting phase occurs. Interestingly, there is an upturn in the resistivity just before the superconducting transition in β-Bi_2Pd. The residual resistivity ratio (ρ_{300K}/ρ_{10K}) for α-BiPd is 177 and for β-Bi_2Pd is 2.6, which is consistent with previous reports [17,33] for both systems and is indicative of good crystalline quality. The upper insets in the (a) and (b) panels of Fig. 12 show the pictures, with attached leads, of the single crystals of α-BiPd and β-Bi_2Pd that were used for transport measurements. The bottom insets in the same panels show the dependence of ρ_{xx} close to the superconducting transition, indicating that T_c for α-BiPd and β-Bi_2Pd crystals is 3.75(5) K and 4.64(5) K, respectively, in agreement with previous reports [17,33]. These values are very close to the ones obtained from the magnetic susceptibility measurements previously shown.

The temperature dependence of resistivity was also determined in the presence of a magnetic field, allowing the upper critical field $\mathbf{H_{c2}(T)}$ of both α-BiPd and β-Bi_2Pd to be estimated (Fig. 13). Experimental data have been analyzed in terms of the phenomenological Ginzburg–Landau (GL) expression $\mathbf{H_{c2}(T)} = \mathbf{H_{c2}}(0)\left[1-(\mathbf{T}/\mathbf{T_c})^2\right]\Big/\left[1+(\mathbf{T}/\mathbf{T_c})^2\right]$, leading to an estimate of $H_{c2}(0)$ equal to 17.2(2) mT and 788(2) mT for α-BiPd and β-Bi_2Pd, respectively.

Hall effect measurements of α-BiPd and β-Bi_2Pd at 2 K have also been performed to determine the behavior of the transverse resistivity ρ_{xy} (Fig. 14). For α-BiPd the current is applied along the *ac* plane and the field is applied along the *b* axis. A purely linear field dependence is

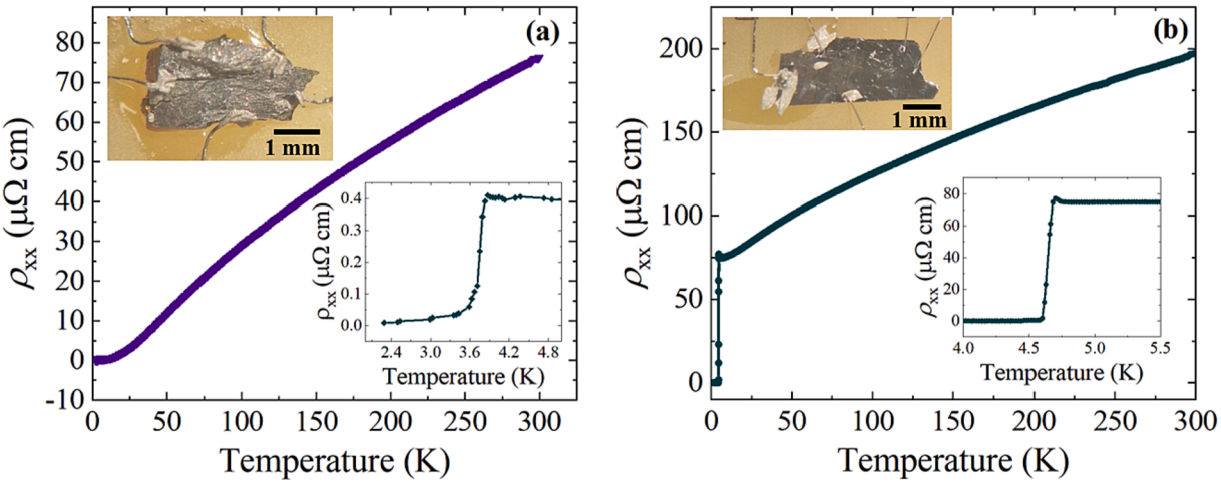

Fig. 12. (a) Transverse resistivity ρ_{xx} as a function of temperature in zero applied field for α-BiPd. Insets show the picture of the measured sample and the dependence ρ_{xx} close to the superconducting transition which is observed at 3.75(5) K. (b) ρ_{xx} as a function of temperature in zero applied field for β-Bi_2Pd. Insets show the picture of the measured sample and the dependence ρ_{xx} close to the superconducting transition which is observed at 4.64(5) K.

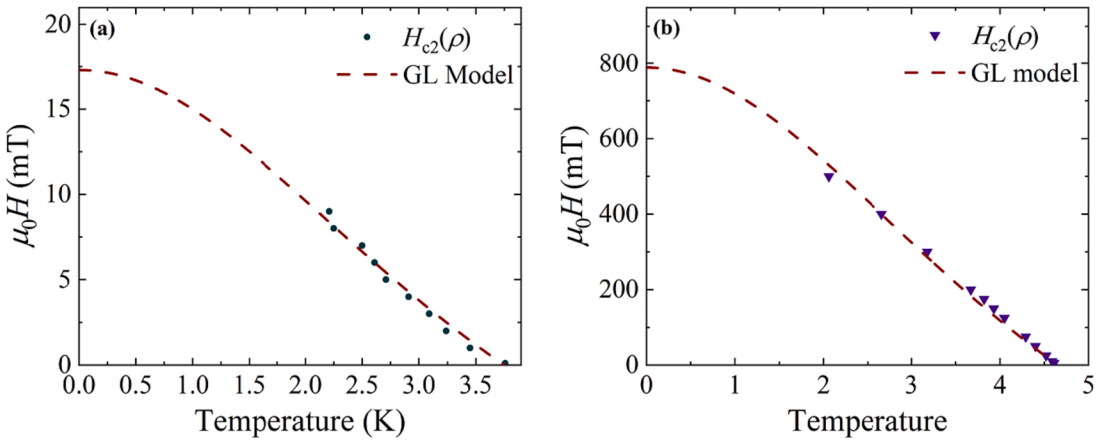

Fig. 13. Upper critical field H_{c2} of (a) α-BiPd and (b) β-Bi_2Pd determined from the 50% point of the superconducting transition measured by electrical resistivity in various applied fields. The upper critical field has been modelled by the Ginzburg-Landau expression giving $H_{c2}(0)$ equal to 17.2(2) and 788 (2) mT for α-BiPd and β-Bi_2Pd, respectively.

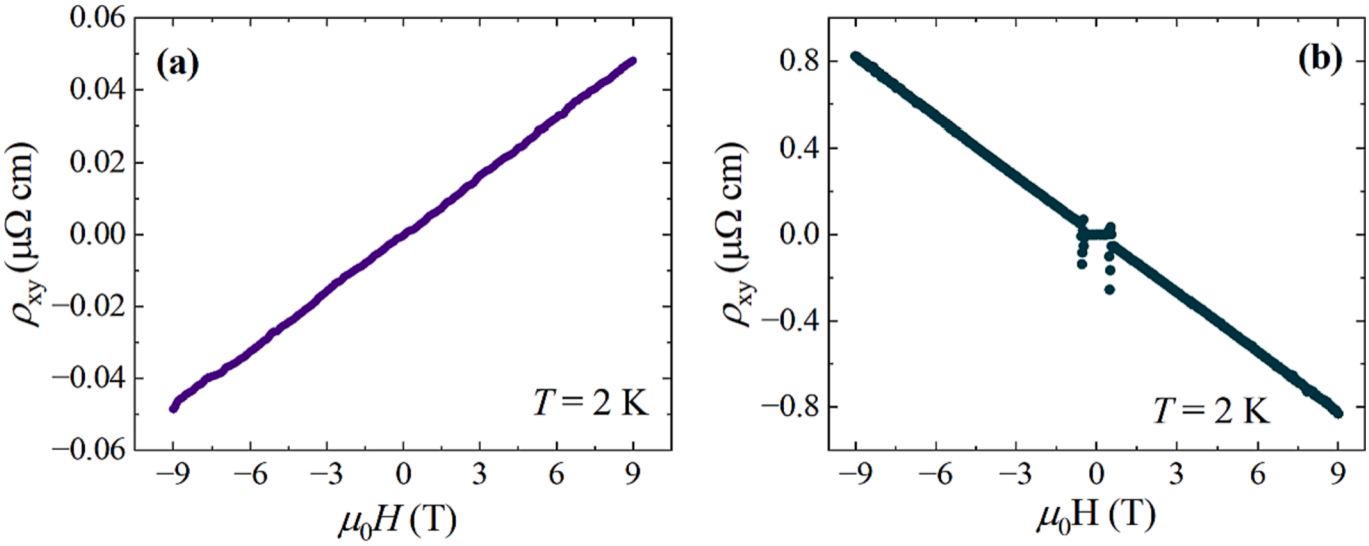

Fig. 14. (a) Field dependence of the longitudinal resistivity ρ_{xy} for α-BiPd at 2 K. (b) Field dependence of ρ_{xy} for β-Bi_2Pd at 2 K.

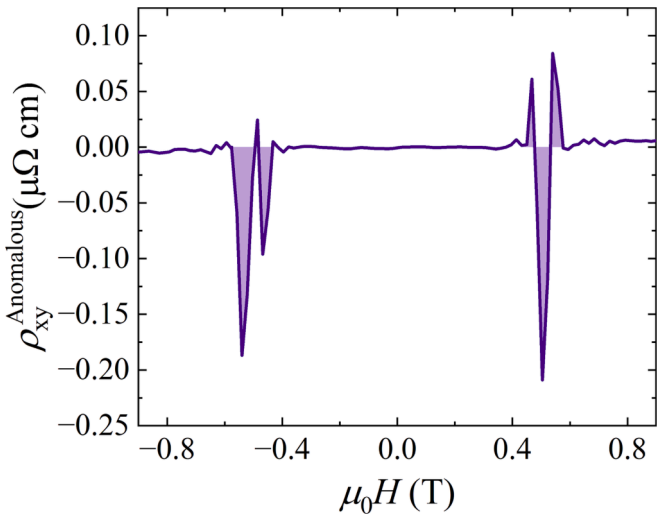

Fig. 15. The leftover anomalous signal in ρ_{xy} for β-Bi_2Pd at 2 K once the ordinary Hall contribution has been subtracted. It is symmetric in field which is not typical of an anomalous Hall effect contribution.

observed indicating that there is only a contribution from the ordinary Hall effect giving a Hall coefficient of 5.35 x 10^{-3} cm/C. For β-Bi_2Pd the current is applied along the *ab* plane while the field is applied along the *c* axis. A linear field dependence is observed above the upper critical field indicating that there is only a contribution from the ordinary Hall effect in this region, with the Hall coefficient found to be equal to −92.3 x 10^{-3} cm/C.

Below the upper critical field an anomalous field dependence is observed. Fig. 15 shows the leftover contribution to the longitudinal resistivity ρ_{xy} once the ordinary Hall effect contribution is subtracted from the signal. Unusually, this leftover signal is symmetric with respect to the field dependence. This effect has previously been observed in β-Bi_2Pd thin films [32] but this is the first observation of this behavior in bulk crystals of Bi_2Pd. In thin films of Bi_2Pd this even in-field ρ_{xy} behavior is postulated to arise from the ratchet effect which originates from asymmetric pinning giving rise to vortex motion. However, in single crystals there is also the possibility of anisotropic resistivity [37] and electronic nematicity [38] giving rise to this effect.

4. Conclusions

α-BiPd and β-Bi_2Pd single crystals have been successfully grown by the floating zone technique using a two-mirror optical floating-zone furnace. The as grown boules are roughly 10–15 mm in length and 6 mm in diameter, from which crystals having size of few millimeters can be selected for experiments. Both α-BiPd and β-Bi_2Pd crystals cleave easily, and the excellent crystallinity of the cleaved surface is confirmed by the quality of the Kikuchi pattern. The presence of twin boundaries in α-BiPd crystals, previously observed with STM/STS experiments, has been revealed for the first time using electron back-scattered diffraction. Next, magnetic susceptibility and resistivity measurements were performed on both types of crystals, along with the determination of the upper critical field. It was verified that the superconducting transition occurred at critical temperature values consistent with the results of previous reports. Finally, Hall effect measurements at 2 K indicated an ordinary Hall effect for the α-BiPd, while an anomalous Hall effect below the upper critical field has been observed in β-Bi_2Pd crystals. This finding, reported up to now only on Bi_2Pd thin films, is observed for the first time in bulk crystals of Bi_2Pd and deserve further study.

CRediT authorship contribution statement

Raja Arumuga: Investigation. **Rosalba Fittipaldi:** Conceptualization, Investigation, Validation, Writing - Original Draft, Supervision, Writing - Review & Editing. **Anita Guarino:** Investigation, Validation, Writing - Original Draft, Writing - Review & Editing. **Daniel Mayoh:** Investigation, Writing - Original Draft. **Alberto Ubaldini:** Investigation. **Mariateresa Lettieri:** Investigation. **Guerino Avallone:** Investigation. **Alfonso Romano:** Writing - Original Draft, Visualization, Writing - Review & Editing. **Geetha Balakrishnan:** Writing – review & editing, Supervision. **Antonio Vecchione:** Writing - Review & Editing, Supervision.

Declaration of Competing Interest

The authors declare that they have no known competing financial interests or personal relationships that could have appeared to influence the work reported in this paper.

Data availability

The data that supports the findings of this study are available in the paper itself.

Acknowledgments

The authors thank Mario Cuoco for helpful discussions. The authors acknowledge C. D'Apolito, I. Immediata, and C. Picarella for technical support. This work was supported in part by the Italian Ministry of Foreign Affairs and International Cooperation, grant number KR23GR06. R.F., A.G., M. L., and A.V. acknowledge the PRIN 2020 project Conquest funded by the Italian Ministry of University and Research (Prot. 2020JZ5N9M).

References

[1] B.Q. Lv, T. Qian, H. Ding, Experimental perspective on three-dimensional topological semimetals, Rev. Mod. Phys. 93 (2021) 025002.
[2] T. Shang, S.K. Ghosh, M. Smidman, D.J. Gawryluk, C.h. Baines, W. An Wang, Y. Xie, M.O. Chen, M. Ajeesh, E. Nicklas, M. Pomjakushina, M. Medarde, J.F. Shi, H. Annett, J.Q. Yuan, T. Shiroka, Spin-triplet superconductivity in Weyl nodal-line semimetals, Npj Quantum Mater. 7 (2022) 35.
[3] V. Mourik, K. Zuo, S.M. Frolov, S.R. Plissard, E.P.A.M. Bakkers, L.P. Kouwenhoven, Signatures of Majorana fermions in hybrid superconductor-semiconductor nanowire devices, Science 336 (2012) 1003.
[4] N.P. Armitage, E.J. Mele, A. Vishwanath, Weyl and Dirac semimetals in three-dimensional solids, Rev. Mod. Phys. 90 (2018) 015001.
[5] B. Joshi, A. Thamizhavel, S. Ramakrishnan, Superconductivity in noncentrosymmetric BiPd, Phys. Rev. B 84 (2011) 064518.
[6] M. Mondal, B. Joshi, S. Kumar, A. Kamlapure, S.C. Ganguli, A. Thamizhavel, S. S. Mandal, S. Ramakrishnan, P. Raychaudhuri, Andreev bound state and multiple energy gaps in the noncentrosymmetric superconductor BiPd, Phys. Rev. B 86 (2012) 094520.
[7] L. Jiao, J.L. Zhang, Y. Chen, Z.F. Weng, Y.M. Shao, J.Y. Feng, X. Lu, B. Joshi, A. Thamizhavel, S. Ramakrishnan, H.Q. Yuan, Anisotropic superconductivity in noncentrosymmetric BiPd, Phys. Rev. B 89 (2014) 060507.
[8] M. Neupane, N. Alidoust, M.M. Hosen, J.-X. Zhu, K. Dimitri, S.-Y. Xu, N. Dhakal, R. Sankar, I. Belopolski, D.S. Sanchez, T.-R. Chang, H.-T. Jeng, K. Miyamoto, T. Okuda, H. Lin, A. Bansil, D. Kaczorowski, F. Chou, M.Z. Hasan, T. Durakiewicz, Observation of the spin-polarized surface state in a noncentrosymmetric superconductor BiPd, Nat. Commun. 7 (2016) 13315.
[9] S. Thirupathaiah, S. Ghosh, R. Jha, E.D.L. Rienks, K. Dolui, V.V. Ravi, B. Kishore, T. Büchner, V.P.S. Das, D.D. Awana, J.F. Sarma, Unusual dirac fermions on the surface of a noncentrosymmetric α-BiPd superconductor, Phys. Rev. Lett. 117 (2016) 177001.
[10] H.M. Benia, E. Rampi, C. Trainer, C.M. Yim, A. Maldonado, D.C. Peets, A. Stöhr, U. Starke, K. Kern, A. Yaresko, G. Levy, A. Damascelli, C.R. Ast, A.P. Schnyder, P. Wahl, Observation of Dirac surface states in the noncentrosymmetric superconductor BiPd, Phys. Rev. B 94 (2016) 121407.
[11] A. Pramanik, R.P. Pandeya, D.V. Vyalikh, A. Generalov, P. Moras, A.K. Kundu, P. M. Sheverdyaeva, C. Carbone, B. Joshi, A. Thamizhavel, S. Ramakrishnan, K. Maiti, Dirac states in the noncentrosymmetric superconductor BiPd, Phys. Rev. B 103 (2021) 155401.
[12] X. Xu, Y. Li, C.L. Chien, Spin-triplet pairing state evidenced by half-quantum flux in a noncentrosymmetric superconductor, Phys. Rev. Lett. 124 (2020) 167001.

[13] Z. Sun, M. Enayat, A. Maldonado, C. Lithgow, E. Yelland, D.C. Peets, A. Yaresko, A. P. Schnyder, P. Wahl, Dirac surface states and nature of superconductivity in noncentrosymmetric BiPd, Nat. Commun. 6 (2015) 6633.
[14] D.C. Peets, A. Maldonado, M. Enayat, Z. Sun, P. Wahl, A.P. Schnyder, Upper critical field of the noncentrosymmetric superconductor BiPd, Phys. Rev. B 93 (2016) 174504.
[15] Y. Imai, F. Nabeshima, T. Yoshinaka, K. Miyatani, R. Kondo, S. Komiya, I. Tsukada, A. Maeda, Superconductivity at 5.4 K in β-Bi_2Pd, J. Phys. Soc. Jpn. 81 (2012) 113708.
[16] K. Iwaya, Y. Kohsaka, K. Okawa, T. Machida, M.S. Bahramy, T. Hanaguri, T. Sasagawa, Full-gap superconductivity in spin-polarised surface states of topological semimetal β-$PdBi_2$, Nature Commun. 8 (2017) 976.
[17] J. Kačmarčík, Z. Pribulová, T. Samuely, P. Szabó, V. Cambel, J. Šoltýs, E. Herrera, H. Suderow, A. Correa-Orellana, D. Prabhakaran, P. Samuely, Single-gap superconductivity in β-Bi_2Pd, Phys. Rev. B 93 (2016) 144502.
[18] M. Sakano, K. Okawa, M. Kanou, H. Sanjo, T. Okuda, T. Sasagawa, K. Ishizaka, Topologically protected surface states in a centrosymmetric superconductor β-$PdBi_2$, Nature Commun. 6 (2015) 8595.
[19] Y.-F. Lv, W.-L. Wang, Y.-M. Zhang, H. Ding, W. Li, L. Wang, K. He, C.-L. Song, X.-C. Ma, Q.-K. Xue, Experimental signature of topological superconductivity and Majorana zero modes on β-Bi_2Pd thin films, Sci. Bull. 62 (2017) 852.
[20] E. Herrera, I. Guillamón, J.A. Galvis, A. Correa, A. Fente, R.F. Luccas, F. J. Mompean, M. García-Hernández, S. Vieira, J.P. Brison, H. Suderow, Magnetic field dependence of the density of states in the multiband superconductor β-Bi_2Pd, Phys. Rev. B 92 (2015) 054507.
[21] L. Che, T. Le, C.Q. Xu, X.Z. Xing, Z. Shi, X. Xu, X. Lu, Absence of Andreev bound states in β-$PdBi_2$ probed by point-contact Andreev reflection spectroscopy, Phys. Rev. B 94 (2016) 024519.
[22] J.J. Zheng, E.R. Margine, Electron-phonon coupling and pairing mechanism in β-Bi_2Pd centrosymmetric superconductor, Phys. Rev. B 95 (2017) 014512.
[23] Springer Handbook of Crystal Growth G. Dhanaraj K. Byrappa V. Prasad M. Dudley (Eds.) Ch. 12 "Crystal Growth of Oxides by Optical Floating Zone Technique" by H. A. Dabkowska A. B. Dabkowski. DOI 10.1007/978-3-540-74761-1.
[24] K.-Z. Du, X. Wang, J. Zhang, X. Liu, C.h. Kloc, Q. Xiong, CdS bulk crystal growth by optical floating zone method: strong photoluminescence upconversion and minimum trapped state emission, Optical Engineering 56 (1) (2017) 011109.
[25] R.D. Zhong, J.A. Schneeloch, T.S. Liu, F.E. Camino, J.M. Tranquada, G.D. Gu, Superconductivity induced by In substitution into the topological crystalline insulator $Pb_{0.5}Sn_{0.5}Te$, Phys. Rev. B 90 (2014) 020505.
[26] S. Cho, B. Dellabetta, A. Yang, J. Schneeloch, Z.h. Xu, T. Valla, G. Gu, M.J. Gilbert, N. Mason, Symmetry protected Josephson supercurrents in three-dimensional topological insulators, Nat. Commun. 4 (2012) 1689.
[27] Y. Bhatt, K. Schubert, Kristallstructur von PdBi.r, J. Less-Common Met. 64 (1979) 17.
[28] N.N. Zhuravlev, Structure of superconductors. X. thermal, microscopic and X-ray investigation of the bismuth-palladium system, Zh. Eksp. Teor. Fiz. 5 (1957) 1064.
[29] D.C. Peets, Crystal growth and upper critical field of the noncentrosymmetric superconductor BiPd, J. Phys.: Conf. Ser. 568 (2014) 022037.
[30] A. Pramanik, R.P. Pandeya, K. Ali, B. Joshi, I. Sarkar, P. Moras, P.M. Sheverdyaeva, A.K. Kundu, C. Carbone, A. Thamizhavel, S. Ramakrishnan, K. Maiti, Depth-resolved core level spectroscopy of noncentrosymmetric solid BiPd, Phys. Rev. B 101 (2020) 035426.
[31] M.A. Khan, D.E. Graf, I. Vekhter, D.A. Browne, J.F. Di Tusa, W.A. Phelan, D. P. Youn, Quantum oscillations and a nontrivial Berry phase in the noncentrosymmetric topological superconductor candidate BiPd, Phys. Rev. B 99 (2019) 020507(R).
[32] X. Xu, Y. Li, C.L. Chien, Anomalous transverse resistance in the topological superconductor β-Bi_2Pd, Nature Comm. 13 (2022) 5321.
[33] J. Juraszek, K. Marcin, K. Dariusz, C. Tomasz, Temperature dependence of the lower critical field of the noncentrosymmetric superconductor α-BiPd, Phys. Status Solidi Rrl 17 (2023) 2200423.
[34] C.M. Yim, C. Trainer, A. Maldonado, B. Braunecker, A. Yaresko, D.C. Peets, P. Wahl, Kinetic stabilization of 1D surface states near twin boundaries in noncentrosymmetric BiPd, Phys. Rev. Lett. 121 (2018) 206401.
[35] V. Randle, Applications of electron backscatter diffraction to materials science: Status in 2009, J. Mater. Sci. 44 (2009) 4211.
[36] A.J. Schwartz M. Kumar B.L. Adams D.P. Field Electron backscatter diffraction in materials science 2009 2nd ed. Springer New York NY.
[37] J. Wu, A.T. Bollinger, X. He, I. Božović, Spontaneous breaking of rotational symmetry in copper oxide superconductors, Nature 547 (2017) 432.
[38] S.J. Hagen, C.J. Lobb, R.L. Greene, M.G. Forrester, J.K. Kang, Anomalous Hall effect in superconductors near their critical temperatures, Phys. Rev. B 41 (1990) 11630.